Applied Mathematics and Computation 236 (2014) 422–436

Contents lists available at ScienceDirect

Applied Mathematics and Computation

journal homepage: www.elsevier.com/locate/amc

On the 2D bioheat equation with convective boundary conditions and its numerical realization via a highly accurate approach

Luciano Bedin [1], Fermín S. Viloche Bazán [*,2]

Department of Mathematics, Federal University of Santa Catarina, 88040-900 Florianópolis, SC, Brazil

ARTICLE INFO

Keywords:
Pennes equation
Convective boundary conditions
Fourier method
Pseudospectral methods

ABSTRACT

A series solution for a 2D bioheat Pennes conduction model with convective boundary conditions is established by using the classical Fourier method. To validate and compare results, a numerical method for constructing highly accurate numerical solutions is also derived and numerically illustrated. Both, the series solution and the proposed numerical method open interesting possibilities of application in inverse perfusion coefficient identification problems.

1. Introduction

Modeling of heat transfer processes in biological tissues is of great importance in therapeutic procedures as well as in temperature-based disease diagnostics. Accurate temperature quantification in these processes is a very difficult task due to several factors peculiar to living tissues, e.g., complex anatomical structure, blood perfusion, etc. [11]. In the context of continuum models, considering the Fourier law and assuming that all heat transfer between the tissue and the blood occurs in the capillaries, the temperature can be obtained by solving the widely used Pennes bioheat transfer equation [28]. Several analytical and numerical methods have been employed to investigate the solution of the bioheat equation in different scenarios. An explicit solution in the case of transient boundary conditions using the Green's function method can be found in [32]; in [8] the authors consider transient coefficients by spectral element methods; oscillatory heat flux condition has been considered in [34] by using the Laplace transform method; in [13] fundamental solutions were obtained in the case of Cartesian, cylindrical and spherical coordinates and in [3] the finite difference method was used in the case of concentric spherical regions (see also [33]). Interesting inverse coefficient estimation problems involving the bioheat equation are addressed in [37,38]. In all the above references only the one dimensional case was analyzed and few papers deal with multiple spatial components. A 2D bioheat transfer model involving convective boundary in a rectangular region has been used in [2] to predict temperature of rectangular perfused organic tissues subjected to hyperthermic treatment. The authors obtained an eigenfunction expansion for the temperature based on an integral transform method for the case where the perfusion coefficient is constant. A 2D rectangular case is also addressed in [6], where the authors employ the radial basis function approach combined with the fundamental solution method to handle spatial discretization.

* Corresponding author.
E-mail addresses: luciano.bedin@ufsc.br (L. Bedin), fermin@mtm.ufsc.br (F.S.V. Bazán).
[1] The work of this author is supported by CNPq, Brazil, Grant 477093/2011-6.
[2] The research of this author is sponsored by CNPq, Brazil, Grants 308709/2011-0, 477093/2011-6.

http://dx.doi.org/10.1016/j.amc.2014.03.071
0096-3003/

The purpose of the present paper is twofold: first, to obtain an explicit Fourier-based solution to the 2D bioheat model subjected to convective boundary conditions in the case of space-wise dependent perfusion coefficient, and second, to introduce a numerical method for constructing highly accurate numerical solutions for the problem under consideration based on the well known pseudospectral collocation (CPS) method. Theoretically, because we deal with a linear second order parabolic equation with mixed boundary conditions on a rectangle, our analysis will be carried out by using the Fourier method. Obviously, alternative approaches such as the semigroup theory [24] or other procedures based on the construction of a suitable heat kernel, are also possible. Our choice for the Fourier method is motivated by its simplicity and as it allows a certain degree of flexibility for treating some particular cases of physical interest, for instance, cases when the perfusion coefficient is space-dependent [37,38], or when both the source term and the perfusion coefficient are constants. Although linear second order parabolic equations are widely discussed in the literature, to the best our knowledge, this approach has not yet been applied to the 2D Pennes model as we described before.

The numerical method we propose is based on the well known pseudospectral collocation Chebyshev method [12,15,27,29,36] in a rectangular domain, which seems appropriate due to its capability of constructing highly accurate numerical solutions. Besides being accurate, another interesting aspect of our numerical method is that it mitigates the well known Gibbs phenomenon occurring at discontinuities, typical of numerical solution constructed by Fourier-based methods. In addition, as we will see our method is much easier to implement than the one described in [8].

The paper is organized as follows. Section 2 describes background information on the bioheat Pennes conduction model, including both the dimensional and non-dimensional forms necessary to describe the physical meaning of the variables involved. In Section 3 we obtain a Fourier series solution for the problem and show the strength of the method in the case when the perfusion coefficient is either space-dependent or constant, illustrating it numerically and testing its validity. Section 4 describes in some details the proposed numerical method as well as a stability analysis that guarantees its efficiency. Numerical results which illustrate the effectiveness of the method are presented and discussed in Section 5. The paper ends with some conclusions in Section 6.

Throughout the paper $L^2(]a,b[\times]c,d[)$ denotes the standard Hilbert space of square-integrable functions in the open rectangle $]a,b[\times]c,d[$, with the scalar product

$$\langle f,g\rangle = \int_a^b \int_c^d fg\, dxdy.$$

2. Pennes equation

The evaluation of temperature fields in biological tissues must take into account complex thermal mechanisms which arise due to microcirculatory blood perfusion, metabolic heat generation, anatomical structure of the tissue, and the heat exchange between the skin and its environment [5,21]. A widely used approach is to regard the tissue as a continuum in which the effects of the presence of a large numbers of vessels are collectively accounted to avoid local anatomical issues [19,11]. In the seminal paper [28], Pennes considered this assumption and introduced the so called bioheat equation

$$\rho c\, \theta_\tau = \nabla\cdot(\kappa\nabla\theta) + h_p + h_m + h_e, \tag{1}$$

where θ stands for the temperature of the tissue, τ is the time variable, ρ, c and κ denote the density, the specific heat and the thermal conductivity of the tissue, respectively; h_e stands for the volumetric rate of external heat and h_m, h_p denote the volumetric rates of metabolic and blood perfusion heat generation, respectively. To obtain (1), Pennes used energy conservation principles assuming that the material is homogeneous and has isotropic thermal properties, as well as the constitutive relation for the heat flux density $\mathbf{h}$ given by the Fourier law for heat conduction

$$\mathbf{h} = -\kappa\nabla\theta. \tag{2}$$

Under the assumption that the blood vessels are isotropic, and that the blood flow enters at arterial temperature but reaches the tissue temperature before leaving the arterial system [31], Pennes concentrated all the perfusion information into the term

$$h_p = w_b c_b(\theta_a - \theta), \tag{3}$$

where θ_a stands for the arterial temperature, c_b denotes the specific heat of the blood and w_b is the so called blood perfusion term which represents the mass flow rate of blood per unit volume of tissue. This means that the volumetric rate of heat generation due to the blood perfusion is proportional to the difference of temperature between the vascular and extra-vascular system. As pointed out in [19], the key assumption in (3) is that the heat transfer between blood vessels and the tissue occurs mainly in the wall of capillaries, where the influence of the thermal effects due to blood velocity can be neglected. The validity of (3) was checked throughout experimental measurements of the temperature in human tissues and the adjustment of w_b until the predicted temperature (solving (1)) agreed well with the measured temperature [19,9,7].

In the present work we consider a rectangular perfused tissue with length and thickness equal to L and 1, respectively. That is to say, the tissue occupies the region $0 \leqslant x^* \leqslant L,\ 0 \leqslant y^* \leqslant 1$, where $(x^*, y^*) \in \mathbb{R}^2$, the boundary $y^* = 1$ represents the upper skin surface, while the boundary $y^* = 0$ corresponds to a wall between the tissue and an adjoint large blood vessel [2].

Thus the transient temperature of the tissue $\theta = \theta(x^*, y^*, \tau)$ is governed by the Pennes bioheat Eq. (1) with convective boundary conditions:

$$\rho c\, \theta_\tau - \kappa \Delta\theta + w_b c_b(\theta - \theta_a) = h_m + h_e, \quad 0 < x^* < L,\ 0 < y^* < 1,\ \tau > 0, \tag{4}$$
$$\theta_{x^*} = 0, \quad x^* = 0,\ 0 < y^* < 1,\ \tau > 0, \tag{5}$$
$$\theta_{x^*} = 0, \quad x^* = L,\ 0 < y^* < 1,\ \tau > 0, \tag{6}$$
$$\kappa\theta_{y^*} = \varsigma(\theta - \theta_\infty), \quad 0 < x^* < L,\ y^* = 0,\ \tau > 0, \tag{7}$$
$$\theta = \theta_b, \quad 0 < x^* < L,\ y^* = 1,\ \tau > 0, \tag{8}$$
$$\theta = \theta_0, \quad 0 < x^* < L,\ 0 < y^* < 1,\ \tau = 0,. \tag{9}$$

In (7), ς denotes the heat transfer coefficient, θ_∞ is the environmental temperature (in the adjacent blood vessel) and θ_b is the skin surface temperature. The convective boundary condition (7) attempts to simulate the heat transfer between the tissue and the adjoint blood vessel in $y^* = 0$, while (5)–(6) are adiabatic conditions. In the upper skin surface, the temperature is prescribed, giving rise to the boundary condition (8). The initial and boundary value problem (4)–(9) very often appears in connection with the modeling of heat transfer processes in tumor hyperthermia and detection of skin burn injury [6,22].

As widely discussed in literature, there are several limitations to be noted regarding the constitutive assumptions in the Pennes bioheat model (1). For instance, the fundamental premise of considering living tissues as a continuum is questioned by several authors [11,16,26]. They argue that a living tissue looks like a fluid saturated porous medium where complex transport phenomena occur, as convection with heat internal generation and mass diffusion. In this vein, generalizations of the standard bioheat transfer model (1) that attempt to simulate the nature of the porous medium have been proposed [25,5]. Unlike the Pennes assumption of homogeneous and isotropic blood flow, in these models the effects of directional convective mechanisms of heat transfer, which depend on the blood velocity (*a priori* known), are taken into account. This is stressed also in [11], where a two-phase microscale approach is considered and the Navier–Stokes equations is used to describe the dynamics of the blood velocity and pressure fields. Another relevant issue regarding the constitutive relations of (1) is the Fourier law (2) for heat conduction in the tissue. When assuming (2), temperature disturbances will be propagated at an infinite speed throughout the medium. But there are evidences of non-Fourier feature in the heat conduction due to the interactions between the blood and the tissue [41,40]. In fact, perturbations in the medium propagate in a finite speed and the thermal wave phenomenon occurs [1]. Then, to take into account the departure of the infinite propagation assumption, (2) is usually replaced by $\mathbf{h} + \tau_r \mathbf{h}_\tau = -\kappa\nabla\theta$, where τ_r is the so called thermal relaxation time [11]. As a consequence, instead of the parabolic Eq. (1) the energy conservation principles give rise to a hyperbolic bioheat transfer equation [39,11,1]. In connection with the above constitutive issues, the assumption (3) for the heat generation due to the blood perfusion is also controversial. Accordingly, modern experimental measurements indicate that, in some cases, a temperature dependent expression for h_p is more appropriate [9,20]. The replacement of h_p in (3) by a temperature dependent expression leads to a nonlinear version of (1), which is referred in [19] to as the *modified Pennes equation*. The temperature dependent expression for h_p accounts for the specificity of each tissue and its response to heat stress; for instance, Lang et al. [20] have considered $h_p = \vartheta(\theta) w_b c_b(\theta_a - \theta)$, where ϑ is an exponential function of the variable θ; Lakhassi et al. [19] in turn, considered h_p as a square function of θ. Numerical results which attempt to compare the constant and the temperature dependent cases can be found in [9].

Although we are aware of the limitations and constitutive issues of the classical bioheat transfer Eq. (1), the extensions and generalized models discussed in the previous paragraph will not be considered here. The reason is that, as pointed out in [41], the Pennes equation has presented good agreement with experimental measurements when applied to a wide class of problems. This is the case, for instance, when the blood perfusion rate must be determined from experimentally measured local temperature gradients [22,38].

We now choose $g_0 > 0$ as a reference source of heating generation, suppose that $\theta_a = \theta_b$ and introduce the following dimensionless variables

$$\begin{aligned} &U = \kappa g_0^{-1} L^{-2}(\theta - \theta_a), \quad M = L^{-1}, \quad (x, y) = L^{-1}(x^*, y^*) \quad t = \kappa\rho^{-1}c^{-1}L^{-2}\tau, \\ &P_f = w_b c_b L^2 \kappa^{-1}, \quad B = \varsigma L \kappa^{-1}, \quad G = (h_e + h_m) g_0^{-1}, \quad U_\infty = \kappa g_0^{-1} L^{-2}(\theta_\infty - \theta_a), \\ &U_0 = \kappa g_0^{-1} L^{-2}(\theta_0 - \theta_a), \end{aligned} \tag{10}$$

to obtain the dimensionless Pennes equation which we will investigate in this work

$$U_t - \Delta U + P_f U = G, \quad 0 < x < 1,\ 0 < y < M,\ t > 0, \tag{11}$$
$$U_x = 0, \quad x = 0,\ 0 < y < M,\ t > 0, \tag{12}$$
$$U_x = 0, \quad x = 1,\ 0 < y < M,\ t > 0, \tag{13}$$
$$U_y = B(U - U_\infty), \quad 0 < x < 1,\ y = 0,\ t > 0, \tag{14}$$
$$U = 0, \quad 0 < x < 1,\ y = M,\ t > 0, \tag{15}$$
$$U = U_0, \quad 0 < x < 1,\ 0 < y < M,\ t = 0. \tag{16}$$

The coefficient P_f in (11) is the so called *perfusion coefficient* which, in general, is time and spacewise-dependent as the tissue is not always homogeneous. Some aspects of the experimental techniques used to estimate P_f can be found in [7,23]. As mentioned before, another approach is to use the Pennes equation in order to obtain P_f numerically from the solution of a suitable inverse problem ([38,37,22]). Here, we consider only the direct problem (11)–(16), in the case where P_f does not depend on time.

For our Fourier analysis of the bioheat problem, the boundary value problem (11)–(16) is first transformed by using auxiliary quantities defined by

$$\xi(y) = \frac{BU_\infty}{M} y(y - M), \tag{17}$$

which clearly satisfies (12)–(15), and

$$f(x,y,t) = G(x,y,t) - P(x,y)\xi(y) + \frac{2BU_\infty}{M}. \tag{18}$$

Elementary analysis then shows that the solution to (11)–(16) can be expressed as $U = V + \xi$, where V solves the transformed problem

$$V_t - \Delta V + P_f V = f, \quad 0 < x < 1,\ 0 < y < M,\ t > 0, \tag{19}$$
$$V_x = 0, \quad x = 0,\ 0 < y < M,\ t > 0, \tag{20}$$
$$V_x = 0, \quad x = 1,\ 0 < y < M,\ t > 0, \tag{21}$$
$$V_y - BV = 0, \quad 0 < x < 1,\ y = 0,\ t > 0, \tag{22}$$
$$V = 0, \quad 0 < x < 1,\ y = M,\ t > 0, \tag{23}$$
$$V = U_0 - \xi, \quad 0 < x < 1,\ 0 < y < M,\ t = 0 \tag{24}$$

which we will use in our Fourier analysis.

3. Fourier series approach

In this section we shall describe the Fourier method to obtain solutions to the initial and boundary value problem (19)–(24). To this end we start by noticing that the standard separation of variables method together with the assumption that we seek solutions of the form $V(x,y,t) = c(t)\psi(x,y)$ lead us to the following eigenvalue problem associated with the elliptic operator $\mathcal{L} := -\Delta + P_f I$

> Find $\lambda \in \mathbb{R}$ and a nontrivial ψ satisfying the boundary conditions (20)–(23) such that
>
> $$\mathcal{L}\psi = \lambda\psi, \quad 0 < x < 1,\ 0 < y < M. \tag{25}$$

We now notice that if P_f is a bounded nonnegative function defined in $]0,1[\times]0,M[$ and $B > 0$, then it can be proved that there exists a non-decreasing sequence of real positive eigenvalues $\{\lambda_k\}_{k=1}^{\infty}$ of $\mathcal{L}$ such that $\lim_{k\to+\infty}\lambda_k = +\infty$ and an orthonormal basis $\{\psi_k\}_{k=1}^{\infty}$ of $L^2(]0,1[\times]0,M[)$ consisting of eigenfunctions of $\mathcal{L}$. This result follows from spectral theory for elliptic operators [10, Theorems 6 and 7 in Appendix D], taking into account the very nature of the boundary conditions (20)–(23) and the convexity of the domain. The key idea is to consider elliptic regularity results on convex polygons [4, Theorems 2.1, 3.2.4 and 3.2.5] in order to show that ψ_k is sufficiently regular such that (25) makes sense. The proofs of these results are outside the scope of the paper and are omitted.

With the existence of families $\{\lambda_k\}_{k=1}^{\infty}, \{\psi_k\}_{k=1}^{\infty}$ ensured, we now seek solutions to (19)–(24) defined by

$$V(x,y,t) = \sum_{k=1}^{+\infty} c_k(t)\psi_k(x,y), \tag{26}$$

where each coefficient $c_k(t)$ is regarded as unknown. Formally, we can differentiate (26) term by term with respect to x, y and t as many times as needed. As a consequence, replacing (26) in (19), recalling the definition of $\mathcal{L}$ and taking into account the equality (25), we get

$$\begin{aligned} &\sum_{k=1}^{+\infty} [c_k'(t) + \lambda_k c_k(t)]\psi_k(x,y) = f(x,y,t), \quad 0 < x < 1,\ 0 < y < M,\ t > 0, \\ &\sum_{k=1}^{+\infty} c_k(0)\psi_k(x,y) = U_0(x,y) - \xi(y), \quad 0 < x < 1,\ 0 < y < M, \end{aligned} \tag{27}$$

for each $k \in \mathbb{N}$. Now, for fixed $j \in \mathbb{N}$, if we multiply (27) by ψ_j, integrate the resulting expression in $[0,1] \times [0,M]$ and use the orthogonality of $\{\psi_k\}_{k=1}^{\infty}$ in $L^2(]0,1[\times]0,M[)$, then we obtain the following initial value problem for c_j

$$\begin{aligned} &c_j'(t) + \lambda_j(t)c_j(t) = f_j(t), \quad t > 0 \\ &c_j(0) = a_j, \end{aligned} \tag{28}$$

where

$$f_j(t) = \int_0^1 \int_0^M f\psi_j dxdy, \quad \text{and} \quad a_j = \int_0^1 \int_0^M (U_0 - \xi)\psi_j dxdy. \tag{29}$$

Elementary calculus shows that the solution of (28) is given by

$$c_j(t) = a_j e^{-\lambda_j t} + \int_0^t f_j(\tau) e^{\lambda_j(\tau - t)} d\tau.$$

Hence we have that

$$V(x,y,t) = \sum_{k=1}^{+\infty} \left(a_k e^{-\lambda_k t} + \int_0^t f_k(\tau) e^{\lambda_k(\tau - t)} d\tau \right) \psi_k(x,y). \tag{30}$$

In order to show that V given in (30) actually satisfies (19)–(23) and matches the initial condition (24), convergence results using suitable norms for the series (30) and its derivatives have to be established. This requires some assumptions on U_0 and f which depend to some extent on the type of solution to (19)–(24) we want. For instance, if $U_0 \in L^2(]0,1[\times]0,M[)$ and f is square-integrable in $]0,1[\times]0,M[\times]0,T[$, (30) is a weak solution of (19)–(24) considering $0 \leqslant t \leqslant T$, as it can be seen following the lines of Chapter III, Section 3 in [18]. More regular solutions to (19)–(24) require smoothness conditions on U_0 and f. When this is the case, a sequence of estimates in a Sobolev spaces setting is required in order to obtain the extra regularity through embedding theorems (see Section 7.1 in [10]). Although this is a standard procedure, there are some difficulties due to the convective boundary conditions and the rectangular domain. However, because one of the main purposes of this is paper is to address the numerical aspects about the construction of (30), the theoretical technicalities in Sobolev space settings are omitted. On the other hand, it is worth noticing that there are situations where $U_0 - \xi$ does not match the conditions (20)–(23) (for example, when U_0 is constant). In these cases, the initial condition (24) is only satisfied in the following average sense: $\lim_{t\to 0^+} \int_0^1 \int_0^M V(x,y,t)\varphi(x,y)dxdy = \int_0^1 \int_0^M (U_0 - \xi)(x,y)\varphi(x,y)dxdy$ for all smooth functions φ defined in $[0,1] \times [0,M]$. The reason of this is that, when $t = 0$, convergence of series (30) holds only in L^2-norm.

The construction of (30) becomes simple when the perfusion coefficient comes in the form $P_f(x,y) = p(x) + q(y)$ with both p and q bounded and nonnegative in $]0,1[\times]0,M[$, as occurs, e.g., in certain inverse problems devoted to the estimation of P_f [2,37]. Of course, applying the separation of variables method to the problem (25), we obtain the following regular Sturm–Liouville problems

$$\begin{aligned} &X''(x) + (\mu^2 - p(x))X(x) = 0, \quad 0 < x < 1 \\ &X'(0) = X'(1) = 0, \end{aligned} \tag{31}$$

$$\begin{aligned} &Y''(y) + (\gamma^2 - q(y))Y(y) = 0, \ 0 < y < M \\ &Y(M) = 0, \quad Y'(0) - BY(0) = 0 \end{aligned} \tag{32}$$

from which the eigenpairs $\{\lambda_k, \psi_k\}$ have to be determined. Arguing as before, there exist nondecreasing sequences $\{\mu_k^2\}_{k=1}^{\infty}$ and $\{\gamma_k^2\}_{k=1}^{\infty}$ of positive eigenvalues for (31) and (32) such that $\lim_{k\to+\infty}\gamma_k = +\infty$, $\lim_{k\to+\infty}\mu_k = +\infty$, with respective eigenfunctions $\widehat{X}_k$ and $\widehat{Y}_k$, such that $\{\widehat{X}_k\}_{k=1}^{\infty}$ and $\{\widehat{Y}_k\}_{k=1}^{\infty}$ are orthonormal basis of $L^2(0,1)$ and $L^2(0,M)$, respectively. It is easy to check that $\{\widehat{X}_i\widehat{Y}_j\}_{i,j=1}^{\infty}$ is an orthonormal basis for $L^2(]0,1[\times]0,M[)$. Obviously, members of $\{\widehat{X}_i\widehat{Y}_j\}_{i,j=1}^{\infty}$ can be enumerated in infinitely many ways and for practical purposes we will consider one of them which picks out low frequencies first. In fact, let us consider an enumeration of $\{\widehat{X}_i\widehat{Y}_j\}_{i,j=1}^{\infty}$ denoted by $\{\psi_k\}_{k=1}^{\infty}$ and obtained through the following procedure:

$$\begin{aligned} &\psi_1 = \widehat{X}_1\widehat{Y}_1, \\ &\psi_2 = \widehat{X}_1\widehat{Y}_2, \quad \psi_3 = \widehat{X}_2\widehat{Y}_1, \\ &\psi_4 = \widehat{X}_1\widehat{Y}_3, \quad \psi_5 = \widehat{X}_2\widehat{Y}_2, \quad \psi_6 = \widehat{X}_3\widehat{Y}_1, \end{aligned} \tag{33}$$

and in general, for given $m \in \mathbb{N}$, $m \geqslant 1$, taking $k = 1 + \frac{m(m-1)}{2}$, we have

$$\psi_k = \widehat{X}_1\widehat{Y}_m, \quad \psi_{k+1} = \widehat{X}_2\widehat{Y}_{m-1}, \ldots, \psi_{k+m-1} = \widehat{X}_m\widehat{Y}_1. \tag{34}$$

Analogously, we let

$$\begin{aligned} &\lambda_1 = \mu_1^2 + \gamma_1^2, \quad \lambda_2 = \mu_1^2 + \gamma_2^2, \quad \lambda_3 = \mu_2^2 + \gamma_1^2, \\ &\lambda_4 = \mu_1^2 + \gamma_3^2, \quad \lambda_5 = \mu_2^2 + \gamma_2^2, \lambda_6 = \mu_3^2 + \gamma_1^2, \ldots. \end{aligned} \tag{35}$$

It is straightforward to check that each ψ_k solves problem (25) considering the respective eigenvalue λ_k. The case $q > 0$ with q constant and $p = 0$ is relatively simple since λ_k and ψ_k can be determined explicitly. Indeed, from elementary calculations it can be seen that

$$\mu_i^2 = (i-1)^2\pi^2, \quad i = 1, 2, \ldots, \tag{36}$$

and that $\gamma_j^2 = \beta_j^2 + q$, where β_j satisfies the non-linear equation:

$$\beta_j \cot(\beta_j M) = -B, \quad j = 1, 2, \ldots. \tag{37}$$

Also, for $i, j \in \mathbb{N}$ the normalized eigenfunctions are proven to be

$$\widehat{X}_i = X_i/N_i, \quad \widehat{Y}_j = Y_j/M_j, \tag{38}$$

where

$$X_i(x) = \cos(\mu_i x), \quad N_i = \left(\int_0^1 X_i^2(x)\,dx\right)^{1/2} = \begin{cases} 1, & \text{if} \quad i = 1 \\ \sqrt{2}/2, & \text{if} \quad i \neq 1 \end{cases} \tag{39}$$

and

$$Y_j(y) = \sin(\beta_j(M-y)), \quad M_j = \left(\int_0^M Y_j^2(y)\,dy\right)^{1/2} = \left(\frac{M}{2} - \frac{1}{4\beta_j}\sin(2\beta_j M)\right)^{1/2}. \tag{40}$$

3.1. Validation of Fourier approach

In order to validate the solution of the bioheat problem (11)–(16) expressed in series form for the constant case $P_f = q > 0$, we shall now describe a numerical example where the source term is defined by

$$G(x,y,t) = e^{at}y^2(y-M)\cos(\pi x)[a\cos(ct) - c\sin(ct)] - e^{at}\cos(ct)\cos(\pi x)[-\pi^2 y^2(y-M) + (6y-2M)] - \frac{2BU_\infty}{M} + P_f\left[e^{at}\cos(ct)y^2(y-M)\cos(\pi x) + \frac{BU_\infty}{M}y(y-M)\right]$$

where a, c are arbitrary real constants, and the initial temperature is

$$U_0(x,y) = y^2(y-M)\cos(\pi x) + \frac{BU_\infty}{M}y(y-M).$$

In this situation, the solution for this bioheat problem can be shown to be

$$U(x,y,t) = e^{at}\cos(ct)y^2(y-M)\cos(\pi x) + \frac{BU_\infty}{M}y(y-M), \tag{41}$$

which, in series form is (see (30))

$$U(x,y,t) = \frac{BU_\infty}{M}y(y-M) + \sum_{\substack{k\in\mathcal{J}_m \\ m\in\mathbb{N},\ m\geqslant 1}}^{\infty} a_k e^{-\lambda_k t}\psi_k(x,y) + \sum_{\substack{k\in\mathcal{J}_m \\ m\in\mathbb{N},\ m\geqslant 1}}^{\infty}\int_0^t f_k(\tau)e^{-\lambda_k(t-\tau)}\psi_k(x,y)d\tau, \tag{42}$$

where $\mathcal{J}_m$ is the set of indexes defined by

$$\mathcal{J}_m = \{\ell \in \mathbb{N}/\ell = m(m-1)/2 + i, \quad i = 1, \ldots, m\} \tag{43}$$

the eigenpairs $\{\lambda_k, \psi_k\}$ are described in (33)–(35) and the coefficients a_k, f_k are given in (29). The main purpose here is to illustrate the accuracy of approximate solutions for the bioheat problem constructed by truncating the series above to a finite number of terms.

For the given data, the coefficients a_k, for given $m \in \mathbb{N}$ and $k = 1 + m(m-1)/2, i \in \{1, \ldots, m\}$, are shown to satisfy

$$a_{k+i-1} = \int_0^1\int_0^M y^2(y-M)\cos(\pi x)\psi_{k+i-1}(x,y)dydx = \begin{cases} 0, & \text{if} \quad i \neq 2 \\ -\frac{\sqrt{2}(M\beta_{m-1}\cos(\beta_{m-1}M) - 3\sin(\beta_{m-1}M) + 2M\beta_{m-1})}{\beta_{m-1}^4 M_{m-1}}, & \text{if} \quad i = 2. \end{cases}$$

In addition, tedious calculations show that the integral in the second sum reduces to 0 if $i \neq 2$, while for $i = 2$ it holds

$$\int_0^t f_{k+1}(\tau)e^{-\lambda_{k+1}(t-\tau)}d\tau = \frac{\sqrt{2}}{2M_{m-1}}e^{-(\mu_2^2+\gamma_{m-1}^2)t}\int_0^t\int_0^M e^{(\mu_2^2+\gamma_{m-1}^2)\tau}(e^{a\tau}y^2(y-M)[a\cos(c\tau) - c\sin(c\tau)] - e^{a\tau}\cos(c\tau)$$
$$[-\pi^2 y^2(y-M) + (6y-2M)] + P_f[e^{a\tau}\cos(c\tau)y^2(y-M)])\sin(\beta_{m-1}(M-y)))dyd\tau.$$

Table 1
Important numbers associated with the series (30) of (41).

j	β_j	$\lambda_{j(j-1)/2+2}$	$a_{j(j-1)/2+2}$	$\overline{f}_{j(j-1)/2+2}$	$a_k e^{-\lambda_k t_f}$
1	1.5803e+00	2.2337e+01	0	0	0
2	4.7156e+00	1.2467e+01	−4.6589e−02	3.8503e−03	−3.8496e−03
3	7.8559e+00	3.2206e+01	−5.0325e−02	8.0945e−05	−8.0239e−05
4	1.0997e+01	7.1685e+01	−6.6664e−03	9.7482e−08	−3.9577e−09
5	1.4138e+01	1.3090e+02	−3.4199e−03	4.7979e−08	−1.4588e−14
6	1.7280e+01	2.0986e+02	−1.2644e−03	1.7739e−08	−7.4777e−22
7	2.0421e+01	3.0856e+02	−8.4292e−04	1.1826e−08	−1.3324e−30
8	2.3563e+01	4.2700e+02	−4.3494e−04	6.1020e−09	−3.5447e−41
9	2.6705e+01	5.6518e+02	−3.2537e−04	4.5647e−09	−2.6381e−53
10	2.9846e+01	7.2310e+02	−1.9814e−04	2.7795e−09	−3.0841e−67
11	3.2988e+01	9.0076e+02	−1.5809e−04	2.2160e−09	−9.1155e−83
12	3.6129e+01	1.0982e+03	−1.0631e−04	1.4853e−09	−4.3817e−100

As a consequence, only the coefficients $a_{j(j-1)/2+2}$, $j \geqslant 1$, play some role in the series (42), and the same observation applies for the f_k. In our computations, the integrals above, which are denoted by $\overline{f}_{k+1}$, and the coefficients f_{k+1} themselves, are all computed by using Gaussian quadrature. The first twelve coefficients a_k and f_k, the corresponding eigenvalues λ_k, as well as the first twelve roots β_j, all of them corresponding to the data

$$a = -50, \quad b = 3\pi, \quad B = 0.015, \quad P_f = 0.1, \quad M = 1, \quad \text{and} \quad U_\infty = 0.001, \tag{44}$$

are displayed in Table 1. From this table, it is apparent that while the eigenvalues λ_k get large for small k, the coefficients a_k decrease with k, becoming fairly small rapidly. A by product of this is that depending on the value of t, the products $a_k e^{-\lambda_k t_f}$ can become fairly small even for small k, as seen in the last column of Table 1, in which the products for $t = t_f = 0.2$ are displayed. Notice that at this value of t, only the first five terms of the series play some role. In other words, from a practical point of view, the final result at $t = 0.2$ will not suffer any modification irrespective of the number of terms (larger than five) being used.

Finally, to evaluate the accuracy of the solution constructed by the Fourier method, introduce the "error" $E(x,y,t) = U(x,y,t) - \widehat{U}(x,y,t)$, where $\widehat{U}(x,y,t)$ denotes the solution constructed by truncating the series (42). Then, for given t, a way to measure the accuracy in $\widehat{U}(x,y,t)$, is by computing any matrix norm [14] of matrix E with entries $\mathrm{E}_{i,j} = E(x_i, y_j, t)$, where (x_i, y_j) are gridpoints on $\mathcal{O}$. For the example under consideration, the error corresponding to a mesh of 21×21 grid points and measured by the matrix 2-norm at $t = 0.2$ is

$$\|\mathrm{E}\|_2 = 1.9827e-08.$$

Numerical results that illustrate the behavior of the approximate solution at $t = 0.2$ and the corresponding error are displayed in Fig. 1.

We close the section by addressing the particular case where the initial temperature and the source term are constant. This case appears in conjunction with inverse problems in cancer therapy [22] where one of the major goals is the identification of the perfusion coefficient P_f from temperature histories of certain rectangular region of organic tissue. Assume that $P_f = q > 0$ and G are constants. Then, after some calculation, we obtain the following solution

$$U(x,y,t) = \eta(y) + \sum_{k=1}^{\infty} a_k e^{-\lambda_k t} \psi_k(x,y), \tag{45}$$

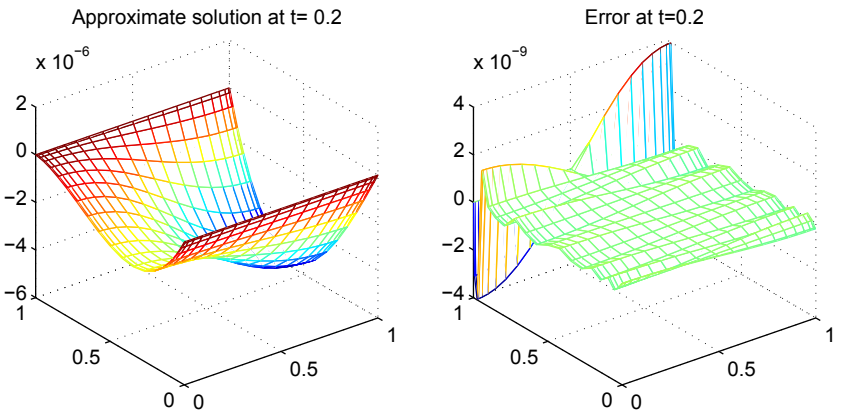

Fig. 1. Approximate solution computed by Fourier method and the "error" $E(x,y,t)$.

where

$$\eta(y) = \frac{G}{q}[1 - \cosh(\sqrt{q}(y - M))] + \frac{BG - BqU_\infty - BG\mathrm{c} - G\sqrt{q}\,\mathrm{s}}{q(\sqrt{q}\,\mathrm{c} + B\mathrm{s})}\sinh(\sqrt{q}(y - M)), \tag{46}$$

with $\mathrm{c} = \cosh(\sqrt{q}M)$, and $\mathrm{s} = \sinh(\sqrt{q}M)$.

Numerical results that illustrate the above statement are postponed to Section 5.

4. Chebyshev pseudoespectral numerical solution

In the previous section we saw that the series solution of the bioheat equation (11)–(16) can be readily computed when the perfusion coefficient is constant. This may no be the case if the eigenvalues and corresponding eigenfuctions are difficult or impossible to determine. In this section we shall consider an alternative approach based on the well known pseudospectral collocation (CPS) method. The CPS approach has become an efficient way to construct approximate solutions to time dependent partial differential equations (PDEs), see, e.g., [27,12,15,17,29,36], due to its high precision and relatively lower computation cost compared with difference finite methods. In this case, the underlying idea is to approximate spatial derivatives by using the differentiation Chebyshev matrix, which gives rise to a system of ordinary differential equations (ODEs) where only the time derivative appears, and then integrate in time by some appropriate numerical scheme for ODEs. For simplicity we shall consider a mesh consisting of $(n+1)\times(n+1)$ grid points on the unit square based on $(n+1)$ Chebyshev-Gauss Lobatto points in each direction:

$$x_i = \frac{1}{2}\left(1 - \cos\frac{\pi i}{n}\right), \quad 0 \leqslant i \leqslant n, \quad y_j = \frac{1}{2}\left(1 - \cos\frac{\pi j}{n}\right), \quad 0 \leqslant j \leqslant n, \tag{47}$$

and assume that the grid points are numbered in the lexicographic ordering, as seen in Fig. 2.

In order to approximate spatial derivatives, let D denote the $(n+1)\times(n+1)$ differentiation Chebysheb matrix in $[0,1]$ and let it be expressed as

$$D = [d_0\ d_1\ \cdots\ d_n] = \begin{bmatrix} r_0^T \\ \vdots \\ r_n^T \end{bmatrix}, \quad d_i, r_i \mathbb{R}^{n+1}. \tag{48}$$

Also, for later use define

$$D_1 = [d_1\ d_2\ \cdots d_{n-1}], \quad D_2 = \begin{bmatrix} r_1^T \\ \vdots \\ r_{n-1}^T \end{bmatrix}. \tag{49}$$

To approximate second order derivatives with respect to x, let

$$\overline{U}_j(t) = [U(x_0, y_j, t), \quad U(x_1, y_j, t), \cdots U(x_n, y_j, t)]^T, \quad 0 \leqslant j \leqslant n. \tag{50}$$

Then, since the second order Chebyshev differentiation matrix, D^2, can be expressed as

$$D^2 = d_0 r_0^T + d_1 r_1^T + \cdots + d_n r_n^T, \tag{51}$$

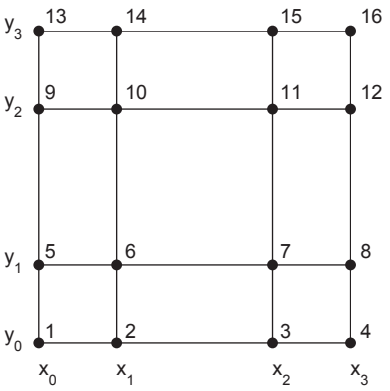

Fig. 2. Grid comprising 16 points corresponding to $n = 3$.

we get

$$\begin{bmatrix} U_{xx}(x_0,y_j,t) \\ U_{xx}(x_1,y_j,t) \\ \vdots \\ U_{xx}(x_n,y_j,t) \end{bmatrix} \approx D^2 \begin{bmatrix} U(x_0,y_j,t) \\ U(x_1,y_j,t) \\ \vdots \\ U(x_n,y_j,t) \end{bmatrix} = d_0 r_0^T \overline{U}_j(t) + D_1 D_2 \overline{U}_j(t) + d_n r_n^T \overline{U}_j(t) \approx D_1 D_2 \overline{U}_j(t), \quad 0 \leqslant j \leqslant n-1, \tag{52}$$

where we have used the fact that $r_i^T \overline{U}_j \approx U_x(x_i,y_j,t)$, the boundary conditions 12,13), and the definitions (49). Therefore, taking the ordering of the grid points into account, we can consider the vector of all unknown on the mesh:

$$\overline{U}(t) = [\overline{U}_0(t)^T \; \overline{U}_1(t)^T \; \cdots \; \overline{U}_{n-1}(t)^T]^T,$$

and use (52) to obtain

$$\begin{bmatrix} U_{xx}(x_0,y_0,t) \\ \vdots \\ U_{xx}(x_n,y_0,t) \\ \vdots \\ U_{xx}(x_0,y_{n-1},t) \\ \vdots \\ U_{xx}(x_n,y_{n-1},t) \end{bmatrix} \approx (I_n \otimes D_1 D_2)\, \overline{U}(t). \tag{53}$$

This completes the approximation of second order derivatives with respect to x in the mesh. Similarly, to approximate second order derivatives with respect to y, for fixed k consider

$$\widetilde{U}_k(t) = [U(x_k,y_0,t), \; U(x_k,y_1,t), \; \cdots \; U(x_k,y_n,t)]^T$$

and use (51) again to obtain

$$\begin{bmatrix} U_{yy}(x_k,y_0,t) \\ U_{yy}(x_k,y_1,t) \\ \vdots \\ U_{yy}(x_k,y_n,t) \end{bmatrix} \approx d_0 r_0^T \widetilde{U}_k(t) + (d_1 r_1^T + \cdots + d_n r_n^T)\widetilde{U}_k(t), \quad 0 \leqslant k \leqslant n. \tag{54}$$

Let $\overline{d}_i$ and $\overline{r}_i$ be the vectors obtained by taking the first n components of d_i and r_i, respectively, and let

$$\overline{D}_1 = [\overline{d}_1 \ldots \overline{d}_n], \quad \overline{D}_2 = \begin{bmatrix} \overline{r}_1^T \\ \vdots \\ \overline{r}_n^T \end{bmatrix}. \tag{55}$$

Then, since $r_0^T \widetilde{U}_k(t) \approx U_y(x_k,y_0,t)$, by virtue of the boundary conditions (14)–(15), we get

$$\begin{bmatrix} U_{yy}(x_k,y_0,t) \\ U_{yy}(x_k,y_1,t) \\ \vdots \\ U_{yy}(x_k,y_{n-1},t) \end{bmatrix} \approx B\,U(x_k,y_0,t)\overline{d}_0 + \overline{D}_1\overline{D}_2 \begin{bmatrix} U(x_k,y_0,t) \\ U(x_k,y_1,t) \\ \vdots \\ U(x_k,y_{(n-1)},t) \end{bmatrix} - B\,U_\infty \overline{d}_0 \approx \left(B\overline{d}_0 e_1^T + \overline{D}_1\overline{D}_2\right) \begin{bmatrix} U(x_k,y_0,t) \\ U(x_k,y_1,t) \\ \vdots \\ U(x_k,y_{(n-1)},t) \end{bmatrix} - B\,U_\infty \overline{d}_0 \tag{56}$$

Based on (56), the vector of second order derivatives with respect to y in all points of the grid can be approximated by

$$\begin{bmatrix} U_{yy}(x_0,y_0,t) \\ \vdots \\ U_{yy}(x_n,y_0,t) \\ \vdots \\ U_{yy}(x_0,y_{n-1},t) \\ \vdots \\ U_{yy}(x_n,y_{n-1},t) \end{bmatrix} \approx \left[\left(B\overline{d}_0 e_1^T + \overline{D}_1\overline{D}_2\right) \otimes I_{(n+1)}\right] \overline{U}(t) - B\,U_\infty \overline{H}, \tag{57}$$

where $\overline{H} = [H_0^T, \ldots, H_{n-1}^T]^T$, with $H_i = e_{i+1}^T \overline{d}_0 [1, \ldots, 1]^T \in \mathbb{R}^{n+1}$, $i = 0, \ldots, n-1$. This completes the discretization of spatial derivatives in the mesh. Now, neglecting discretization errors and denoting the vector of approximations to $\overline{U}(t)$ by $W(t)$, combination of (53), (57) and (11) yields an initial-value problem for a system of linear ordinary differential equations of the form

$$\begin{cases} W'(t) = AW(t) + S(t), \\ W(0) = U_0, \end{cases} \tag{58}$$

where

$$A = \left[(I_n \otimes D_1 D_2) + (B\overline{d}_0 e_1^T + \overline{D}_1 \overline{D}_2) \otimes I_{(n+1)} - \overline{P}_f \right], \tag{59}$$

$$\overline{P}_f = \operatorname{diag}\big(P_f(x_0, y_0), \ldots, P_f(x_n, y_0), \ldots, P_f(x_0, y_{n-1}), \ldots, P_f(x_n, y_{n-1})\big), \tag{60}$$

and

$$S(t) = \overline{F}(t) - BU_\infty \overline{H}, \tag{61}$$

with

$$\overline{F}(t) = [F(x_0, y_0, t), \ldots, F(x_n, y_0, t), \ldots, F(x_0, y_{n-1}, t), \ldots, F(x_n, y_{n-1}, t)]^T. \tag{62}$$

It should be noticed that the solution to the initial-value problem (58) is

$$W(t) = e^{At} W(0) + \int_0^t e^{A(t-\tau)} S(\tau) d\tau \tag{63}$$

and that it can be computed using eigenvalues and eigenvectors of A.

The capability of the CPS method to produce highly accurate numerical solutions relies on the fact that accurate approximation to the most important features of the EDP, namely the eigenvalues λ_k and eigenmodes ψ_k, are now concentrated in the eigensystem of matrix A. To illustrate this, the first 100 eigenvalues of the continuous problem as well as their approximations obtained from matrix A for $n = 30$, are displayed in Fig. 3.

To illustrate something similar with regard to eigenmodes, the first four continuous eigenmodes and the first four discrete eigenmodes, for the same data set given in (44), are all displayed in Fig. 4. Note that for $n = 30$, three of the continuous eigenmodes are already captured.

Summarizing, the CPS-based numerical approach for computing approximate solutions to the initial and boundary value problem involving the bioheat equation reduces to apply time integration methods for ODEs, like multi-step or Runge–Kutta methods, for solving the initial value problem (58). In our computations we integrate in time by the fourth order Runge–Kutta method which we denote by **CPS-RK4**. If we let V_k denote the value that approximates $V(t_k)$, $t_k = \Delta t\, k$, the method can be outlined as follows:

CPS-RK4:
For $k \geqslant 0$, calculate

$$W_{k+1} = W_k + \frac{\Delta t}{6}(F_1 + 2F_2 + 2F_3 + F_4), \tag{64}$$

where

$$F_1 = AW_k + S(t_k), \quad F_2 = A\left(W_k + \frac{\Delta t}{2} F_1\right) + S\left(t_k + \frac{\Delta t}{2}\right)$$
$$F_3 = A\left(W_k + \frac{\Delta t}{2} F_2\right) + S\left(t_k + \frac{\Delta t}{2}\right), \quad F_4 = A(W_k + \Delta t F_3) + S(t_{k+1}).$$

4.1. Stability considerations

This section is concerned with the problem of determining the maximum stepsize for **RK4** which will assure stable integration of the system of ODEs (58). Regarding this, it is well known that for ODEs of the form (58) with system matrix A, close to normal, the stepsize Δt has to be chosen is such a way that

$$\Delta t\, \Lambda(A) \subset \mathcal{S}, \tag{65}$$

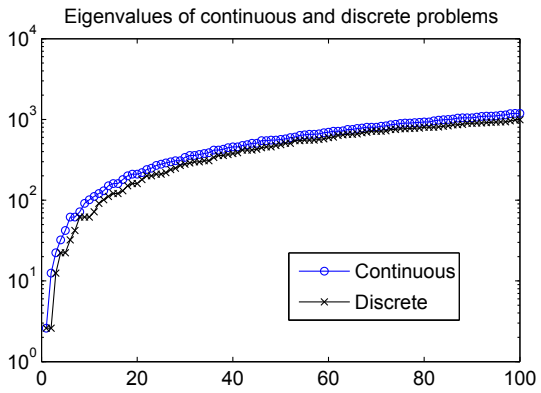

Fig. 3. Eigenvalues of continuous and discrete problems for the data set described in (44).

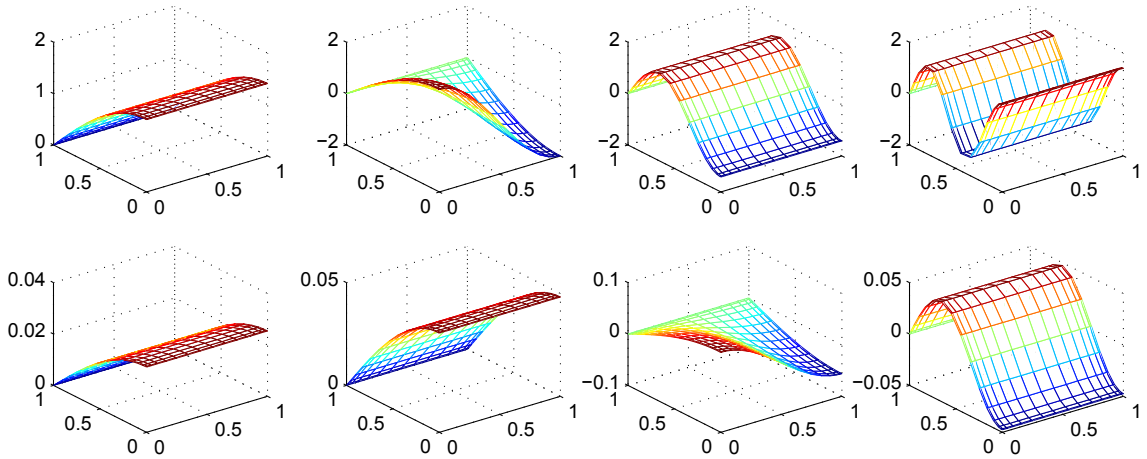

Fig. 4. First four eigenmodes of continuous (top) and discrete (bottom) Bioheat problems.

where $\Lambda(A)$ denotes the spectrum of A and $\mathcal{S}$ denotes the stability region of the time integrator. As far as **RK4** is concerned, based on the fact that the left end of the interval of absolute stability for this method is known to be approximately 2.78, it then follows that the maximum timestep can be calculated by the formula

$$\Delta t_{\max} = \frac{2.78}{\rho(A)}, \tag{66}$$

where $\rho(A)$ denotes the spectral radius of A. Since the system matrix of the bioheat equation depends only on the constant B and on the perfusion coefficient, P_f, see (59), the maximum timestep will depend on these quantities as well. As an example, the maximum timestep determined by the eigenvalue analysis for several values of n, for the case P_f constant, is displayed in Table 2. These values correspond to $P_f = 0.1$ and $B = 0.015$.

However, it is also known that for non normal matrices the above stability condition is not always reliable and frequently seen to fail when the system matrix is far from normal. Indeed, as demonstrated and numerically illustrated in [30,35], in

Table 2
Maximum timestep for stable integration of the bioheat problem via **RK4**.

n	$\Delta t_{\max}$
4	0.018513330978850
8	0.001591237648635
16	0.000108769056027
24	0.000021833578083
32	0.000006946990495
64	0.000000436523827

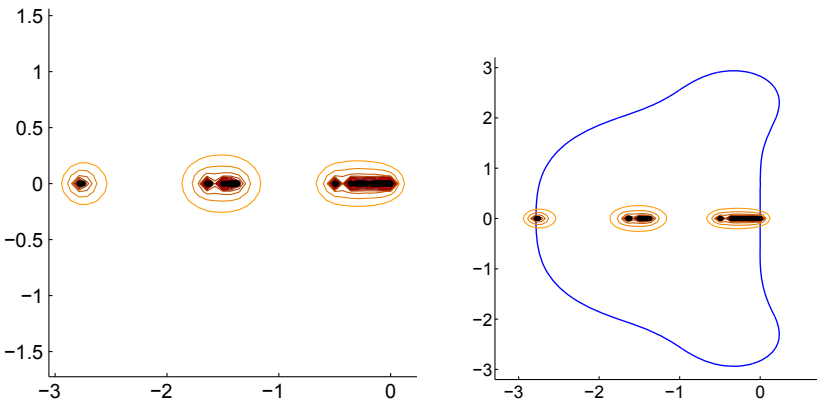

Fig. 5. ϵ-Pseudospectra of matrix A for $\epsilon = 10^{-1}, 10^{-2} \ldots, 10^{-5}, n+1 = 25$, (left) and region of absolute stability of **RK4** scaled by Δt (right) with Δt defined in (66).

these cases the maximum timestep must be chosen in such a way that the ϵ-pseudospectrum of $\Delta t A$ lie within a distance $0(\epsilon) + 0(\Delta t)$ of the stability region as both ϵ and Δt remain small enough. The spectrum and pseudospectra of matrix A for $n = 24$ and $\Delta t\,\mathcal{S}$, the scaled region of absolute stability of **RK4** with Δt shown in Table 2, are displayed in Fig. 5. Since with this Δt the ϵ-pseudospectra of A fall well inside the scaled region of absolute stability for small ϵ, it can be concluded that both the pseudoeigenvalue and the eigenvalue criteria are actually satisfied and therefore, the stability limits on timestep Δt for stable integration determined by the spectral radius of A is appropriate in this case; the same holds for other values of n.

5. Numerical examples

We now numerically illustrate the effectiveness of the CPS-based approach when applied to our bioheat model. Three examples are considered and implemented using MATLAB.

Example 1. We consider the bioheat problem using the data set (44). The purpose is to compare the accuracy of the numerical solution obtained by the Fourier method against the one obtained by **CPS-RK4**. To this end, we take $n = 20$, which implies a grid of 21×21 points and a system matrix A of size 420×420, and run **CPS-RK4** using a timestep $\Delta t = 0.00004$. The results are displayed in Fig. 6. Comparing the " error surface" obtained via **CPS-RK4** with that obtained using the Fourier method (see Fig. 1), we see that the superiority of **CPS-RK4** in terms of accuracy is apparent.

Example 2. The goal of this example is to assess the quality of approximate solutions obtained by both the Fourier method and **CPS-RK4** for the case where the initial temperature U_0, the source term G, and the perfusion coefficient P_f are all constant, and therefore the exact solution to the bioheat problem is not available. In this case, the perfusion coefficient is set to $P_f = 4.5$, the initial temperature is $U_0 = 0.05$, and the source term is $G = 0.25$. The rest of parameters are the same as in (44). With regard to the solution in series form, note that only the coefficients a_k and corresponding eigenmodes are required. In this case, for each $m \in \mathbb{N}, k = 1 + m(m-1)/2$ and $i \in \{1, \ldots, m\}$, it follows that

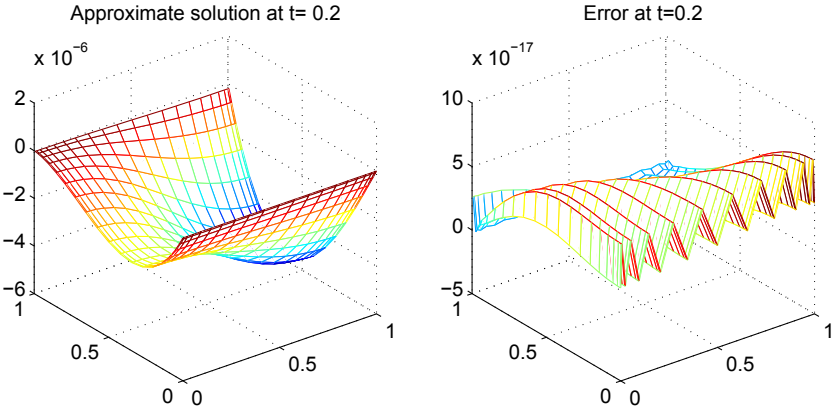

Fig. 6. Approximate solution computed by **CPS-RK4** and corresponding error with respect to the exact solution in a grid of 21×21 points.

$$a_{k+i-1} = \int_0^1 \int_0^M (U_0 - \eta(y)))\psi_{k+i-1}(x,y)dydx = T_0 \int_0^1 \int_0^M \widehat{X}_i(x)\widehat{Y}_{m-i+1}(y)dydx - \int_0^1 \int_0^M \eta(y)\widehat{X}_i(x)\widehat{Y}_{m-i+1}(y)dydx$$

After some calculations we get

$$a_{k+i-1} = \begin{cases} 0, & \text{if} \quad i \neq 1 \\ \frac{U_0}{\beta_m M_m}(\cos(\beta_m M) - 1) - \frac{1}{M_m}\int_0^M \eta(y)\sin(\beta_m(M-y))dy, & \text{if} \quad i = 1. \end{cases}$$

This shows that only the coefficients of the form $a_{j(j-1)/2+1}, j \geqslant 1$, as well as the corresponding eigenmodes, are required to construct the solution in series form. Having stated this, the sought coefficients are computed by using Gaussian quadrature and the sum is performed as in the example of the previous section but now at two time levels, the first one at $t = 0.00004$ and the other one at $t = 0.1$. In addition, **CPS-RK4**-based solutions using $n + 1 = 21$ grid points are also computed. The results for $t = 0.00004$ are displayed in Fig. 7 (first row).

In this case we note that the Fourier-based solution starts to oscillate near the boundary, thus confirming the well-known Gibbs phenomenon attributed to the Fourier method in the presence of discontinuities, and that the **CPS-RK4**-based solution does not suffer from these difficulties. The solutions corresponding to the time level $t = 0.1$, displayed in Fig. 7 (second row), show that both methods calculate essentially the "same solution".

Example 3. Spatial-dependent Perfusion coefficient case

We now illustrate the effectiveness of **CPS-RK4** with two examples where the coefficient P_f is nonsmooth and dependent on x. In these cases, the source term $G(x,y)$ is chosen so that the solution $U(x,y)$ of the bioheat problem is the function defined in (41), where a, b, B, M and U_∞ are the same as in (44), and where the perfusion coefficient for each case is as in Fig. 8.

The results of the experiment for the case where $n = 20$ and the perfusion coefficient is as in Fig. 8 (right) are displayed in Fig. 9. The results for the other case were very similar and are not included here.

6. Conclusions

A two dimensional Pennes equation subjected to mixed boundary conditions in a rectangle was considered. Using the Fourier method we obtain the solution of this problem explicitly in terms of a series depending on the eigenfunctions

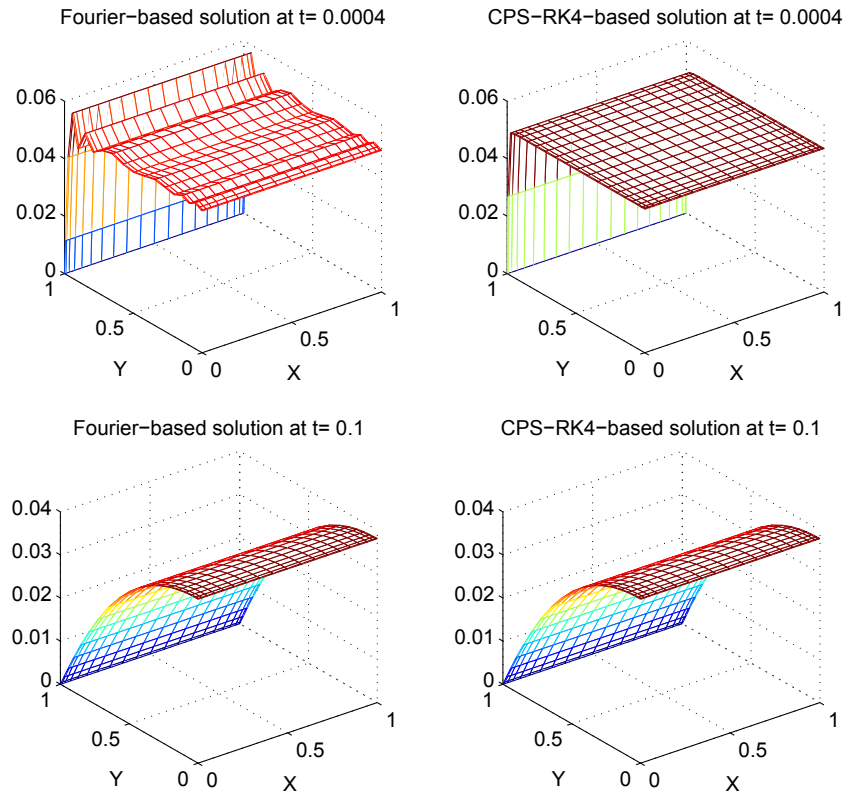

Fig. 7. Approximate solution computed by Fourier and CPS-RK4 methods on a grid of 21×21 points at two time levels.

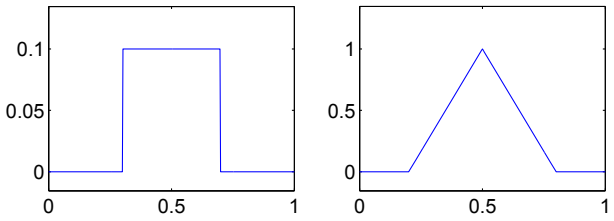

Fig. 8. Nonsmooth space-dependent perfusion coefficient $P_f(x)$.

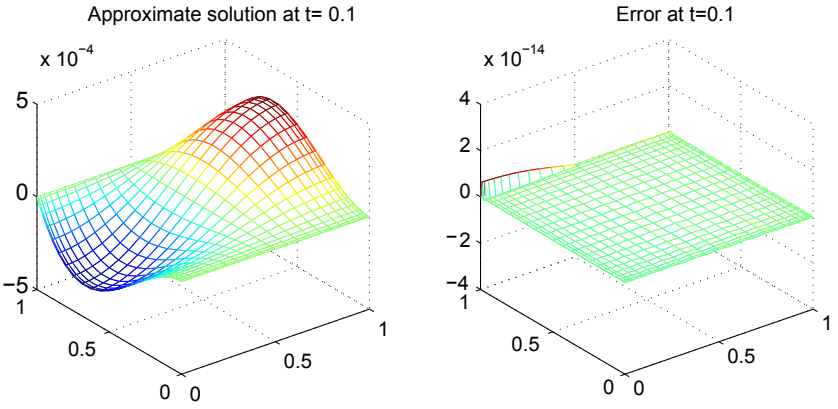

Fig. 9. Numerical results for spatial-dependent perfusion coefficient case.

and eingenvalues of the elliptic operator $\mathcal{L}$. Numerical results showed that convergence of the series can be very fast provided the solution satisfies certain smoothness condition. Further, to assess the accuracy of the solution expressed in series form, we introduced a pseudospectral numerical method capable of constructing highly accurate numerical solutions. The method was illustrated numerically and its efficiency verified. Finally, the authors believe that the theory and the numerical method can serve as the basis for new methods in inverse perfusion coefficient estimation problems. This is the subject of ongoing research.

References

[1] H. Ahmadikia, R. Fazlali, A. Moradi, Analytical solution of the parabolic and hyperbolic heat transfer equations with constant and transient heat flux conditions on skin tissue, Int. Commun. Heat Mass Transfer 39 (2012) 121–130.
[2] M.D.B. Azevedo, R.O.C Guedes and F. Scofano Neto, Analytical solution to the two dimensional transient bioheat equation with convective boundary conditions, Proceedings of the 11 ENCIT, Paper CIT06-0605, 2006.
[3] H.G. Bagaria, D.T. Johnson, Transient solution to the bioheat equation and optimization for magnetic fluid hyperthermia treatment, Int. J. Hyperther. 21 (2005) 57–75.
[4] J. Banasiak, G.F. Roach, On mixed boundary value problems of Dirichlet oblique-derivative type in plane domains with piecewise differentiable boundary, J. Differ. Equ. 79 (1989) 111–131.
[5] A. Belmiloudi, Parameter identification problems and analysis of the impact of porous media in biofluid heat transfer in biological tissues during thermal therapy, Nonlinear Anal. Real World Appl. 11 (2010) 1345–1363.
[6] L. Cao, Q. Qin, N. Zhao, An RBF-MFS model for analysing thermal behaviour of skin tissues, Int. J. Heat Mass Transfer 53 (2010) 1298–1307.
[7] A.V. Cardinali, Validation of a Noninvasive Blood Perfusion Measurement Sensor. Master Thesis in Mechanical Engineering, Faculty of the Virginia Polytechnic Institute and State University, 2002.
[8] M. Deghan, M. Sabouri, A spectral element method for solving the Pennes bioheat transfer equation by using triangular and quadrilateral elements, App. Math. Modell. 36 (2012) 6031–6049.
[9] T. Drisdal, P. Togni, L. Visek, J. Vrba, Comparison of constant and temperature dependent blood perfusion in temperature prediction for superficial hyperthermia, Radioengineering 19 (2010) 281–289.
[10] L.C. Evans, Partial Differential Equation, AMS, 1998.
[11] J. Fan, L. Wang, Analytical theory of bioheat transport, J. Appl. Phys. 109 (2011) 1–43.
[12] B. Fornberg, A Practical Guide to Pseudospectral Methods, Cambridge University Press, Cambridge, 1996.
[13] M. Giordano, G. Gutierrez, C. Rinaldi, Fundamental solutions to the bioheat equation and their application to magnetic fluid hyperthermia, Int. J. Hyperther. 26 (5) (2006) 475–484.
[14] G.H. Golub, C.F. Van Loan, Matrix Computations, 3rd ed., Johns Hopkins University Press, Baltimore, 1996.
[15] D. Gotlieb, S.A. Orzag, Numerical Analysis of Spectral Methods: Theory and Practice, SIAM, Philadelphia, PA, 1977.
[16] A.R.A. Khaled, K. Vafai, The role of porous media in modeling flow and heat transfer in biological tissues, Int. J. Heat Mass Transfer 46 (2003) 4989–5003.
[17] D. Kosloff, H. Tal, Ezer, Modified Chebyshev pseudospectral method with $O(N^{-1})$ time step restriction, J. Comput. Phys. 104 (1993) 457–469.
[18] O.A. Ladyzhenskaya, The Boundary Value Problems of Mathematical Physics, Springer-Verlag, 1985.

[19] A. Lakhssassi, E. Kengne, H. Semmaoui, Modified Pennes' equation modelling bioheat transfer in living tissues: analytical and numerical analysis, Nat. Sci. 2 (2010) 1375–1385.
[20] J. Lang, B. Erdmann, M. Seebass, Impact of nonlinear heat transfer on temperature control in regional hyperthermia, IEEE Transaction on Biomedical Engineering 46 (1999) 1129–1138.
[21] J. Liu, L.X. Xu, Boundary information based diagnostics on the thermal states of biological bodies, Int. J. Heat Mass Transfer 43 (2000) 2827–2839.
[22] C.F. Lopes, M.V.C. Souza, F. Scofano Neto, M.J. Colaço, A.B. Caldeira R.O.C. Guedes, Inverse problem of estimation of the blood perfusion coefficient in cancerous tissues subjected to Hyperthermic treatments, in: EngOpt 2008- International Conference on Engineering Optimization, Rio de Janeiro, 2008.
[23] L. Lüdemann, P. Wust, J. Gellermann, Perfusion measurement using DCE-MRI: implication for hyperthermia, Int. J. Hyperther. 24 (2008) 91–96.
[24] A. Lunardi, Analytic Semigroups and Optimal Regularity in Parabolic Problems, Birkhäuser, 1995.
[25] A. Nakayama, F. Kuwahara, A general bioheat transfer model based on the theory of porous media, Int. J. Heat Mass Transfer 51 (2008) 3190–3199.
[26] D.A. Nield, A.V. Kuznetsov, A bioheat transfer model: forced convection in a channel occupied by a porous medium with counterflow, Int. J. Heat Mass Transfer 51 (2008) 5534–5541.
[27] J.C. Oliveira, F.S.V. Bazán, Poisson approach for evaluating numerical methods for the two-dimensional wave equation constrained to absorbing boundary conditions, Appl. Math. Comput. 209 (2009) 273–284.
[28] H.H. Pennes, Analysis of tissue and arterial blood temperatures in the resting human forearm, J. Appl. Physiol. 1 (2) (1948) 93–122.
[29] A. Quarteroni, A. Valli, Numerical Approximation of Partial Differential Equations, Springer, 1997.
[30] S. Reddy, N. Trefethen, Stability analysis of the method of lines, Numer. Math. 62 (1992) 237–267.
[31] R.M. Romero, J.J. Lozano, M. Sen, F. Gonzalez, Analytical solution of the Pennes equation for burn depth determination from infrared thermographs, Math. Med. Biol. 27 (2009) 21–38.
[32] K.A. Shah, P.H. Bhathawala, Analytical solution of malignant skin tumor problem by Green's function method, Int. J. Appl. Math. Mech. 8 (17) (2012) 98–111.
[33] W. Shen, J. Zhang, Modeling and numerical simulation of bioheat transfer and biomechanics in soft tissue, Math. Comput. Model. 41 (2005) 1251–1265.
[34] T.C. Shih, Y. Ping, W. Lin, H. Kou, Analytical analysis of the Pennes bioheat transfer equation with sinusoidal heat flux condition on skin surface, Med. Eng. Phys. 29 (2007) 946–953.
[35] L.N. Trefethen, M. Embree, Spectra and Pseudospectra – The Behavior of Nonnormal Matrices and Operators, Princeton University Press, Princeton, 2005.
[36] L.N. Trefethen, Spectral Methods in Matlab, SIAM, Philadelphia, PA, 2000.
[37] D. Trucu, D.B. Ingham, D. Lesnic, Inverse time-dependent perfusion coefficient identification, J. Phys. Conf. Ser. 124 (2008) 012050.
[38] D. Trucu, D.B. Ingham, D. Lesnic, Space-dependent perfusion coefficient identification in the transient bio-heat equation, J. Eng. Math. 67 (2010) 307–315.
[39] M.M. Tung, M. Trujillo, J.A. López Molina, M.J. Rivera, E.J. Berjano, Modeling the heating of biological tissue based on the hyperbolic heat transfer equation, Math. Comput. Model. 50 (2009) 665–672.
[40] F. Xu, K.A. Seffen, T.J. Lu, Non-Fourier analysis of skin biothermomechanics, Int. J. Heat Mass Transfer 51 (2008) 2237–2259.
[41] Y. Zhang, Generalized dual-phase lag bioheat equations based on nonequilibrium heat transfer in living biological tissues, Int. J. Mass Heat Transfer 52 (2009) 4829–4834.